

Chapter 2

Superconducting magnet

2.1 Overview

The superconducting magnet for CMS [3–6] has been designed to reach a 4-T field in a free bore of 6-m diameter and 12.5-m length with a stored energy of 2.6 GJ at full current. The flux is returned through a 10 000-t yoke comprising 5 wheels and 2 endcaps, composed of three disks each (figure 1.1). The distinctive feature of the 220-t cold mass is the 4-layer winding made from a stabilised reinforced NbTi conductor. The ratio between stored energy and cold mass is high (11.6 KJ/kg), causing a large mechanical deformation (0.15%) during energising, well beyond the values of previous solenoidal detector magnets. The parameters of the CMS magnet are summarised in table 2.1. The magnet was designed to be assembled and tested in a surface hall (SX5), prior to being lowered 90 m below ground to its final position in the experimental cavern. After provisional connection to its ancillaries, the CMS Magnet has been fully and successfully tested and commissioned in SX5 during autumn 2006.

2.2 Main features of the magnet components

2.2.1 Superconducting solenoid

The superconducting solenoid (see an artistic view in figure 2.1 and a picture taken during assembly in the vertical position in SX5 in figure 2.2) presents three new features with respect to previous detector magnets:

- Due to the number of ampere-turns required for generating a field of 4 T (41.7 MA-turn), the winding is composed of 4 layers, instead of the usual 1 (as in the Aleph [7] and Delphi [8] coils) or maximum 2 layers (as in the ZEUS [9] and BaBar [10] coils);
- The conductor, made from a Rutherford-type cable co-extruded with pure aluminium (the so-called insert), is mechanically reinforced with an aluminium alloy;
- The dimensions of the solenoid are very large (6.3-m cold bore, 12.5-m length, 220-t mass).

For physics reasons, the radial extent of the coil (ΔR) had to be kept small, and thus the CMS coil is in effect a “thin coil” ($\Delta R/R \sim 0.1$). The hoop strain (ϵ) is then determined by the

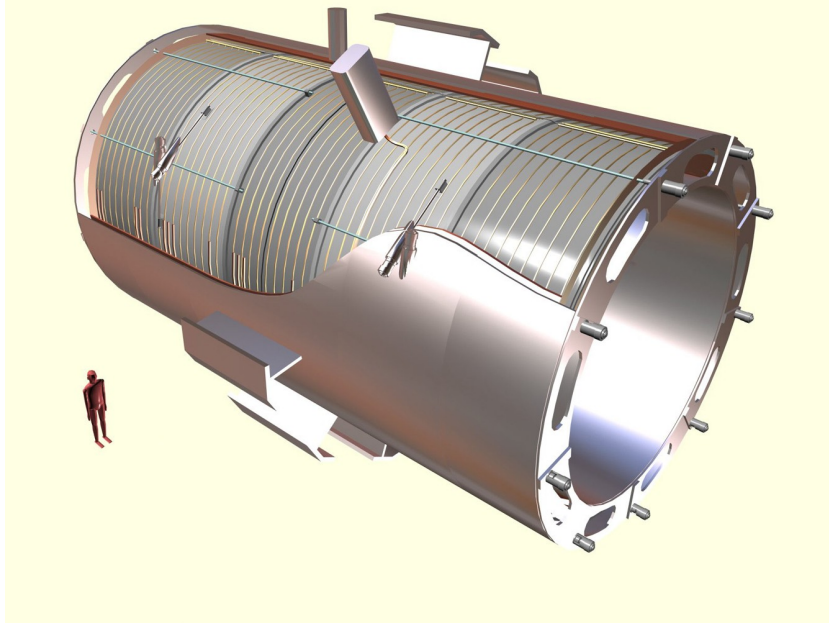


Figure 2.1: General artistic view of the 5 modules composing the cold mass inside the cryostat, with details of the supporting system (vertical, radial and longitudinal tie rods).

magnetic pressure ($P = \frac{B_0^2}{2\mu_0} = 6.4$ MPa), the elastic modulus of the material (mainly aluminium with $Y = 80$ GPa) and the structural thickness ($\Delta R_s = 170$ mm i.e., about half of the total cold mass thickness), according to $\frac{PR}{\Delta R_s} = Y\varepsilon$, giving $\varepsilon = 1.5 \times 10^{-3}$. This value is high compared to the strain of previous existing detector magnets. This can be better viewed looking at a more significant figure of merit, i.e. the E/M ratio directly proportional to the mechanical hoop strain according to $\frac{E}{M} = \frac{PR}{2\Delta R_s \delta} \frac{\Delta R_s}{\Delta R} = \frac{\Delta R_s Y \varepsilon}{\Delta R 2\delta}$, where δ is the mass density. Figure 2.3 shows the values of E/M as function of stored energy for several detector magnets. The CMS coil is distinguishably far from other detector magnets when combining stored energy and E/M ratio (i.e. mechanical deformation). In order to provide the necessary hoop strength, a large fraction of the CMS coil must have a structural function. To limit the shear stress level inside the winding and prevent cracking the insulation, especially at the border defined by the winding and the external mandrel, the structural material cannot be too far from the current-carrying elements (the turns). On the basis of these considerations, the innovative design of the CMS magnet uses a self-supporting conductor, by including in it the structural material. The magnetic hoop stress (130 MPa) is shared between the layers (70%) and the support cylindrical mandrel (30%) rather than being taken by the outer mandrel only, as was the case in the previous generation of thin detector solenoids. A cross section of the cold mass is shown in figure 2.4.

The construction of a winding using a reinforced conductor required technological developments for both the conductor [11] and the winding. In particular, for the winding many problems had to be faced mainly related to the mandrel construction [12], the winding method [13], and the module-to-module mechanical coupling. The modular concept of the cold mass had to face the problem of the module-to-module mechanical connection. These interfaces (figure 2.5) are critical

Table 2.1: Main parameters of the CMS magnet.

General parameters	
Magnetic length	12.5 m
Cold bore diameter	6.3 m
Central magnetic induction	4 T
Total Ampere-turns	41.7 MA-turns
Nominal current	19.14 kA
Inductance	14.2 H
Stored energy	2.6 GJ
Cold mass	
Layout	Five modules mechanically and electrically coupled
Radial thickness of cold mass	312 mm
Radiation thickness of cold mass	$3.9 X_0$
Weight of cold mass	220 t
Maximum induction on conductor	4.6 T
Temperature margin wrt operating temperature	1.8 K
Stored energy/unit cold mass	11.6 kJ/kg
Iron yoke	
Outer diameter of the iron flats	14 m
Length of barrel	13 m
Thickness of the iron layers in barrel	300, 630 and 630 mm
Mass of iron in barrel	6000 t
Thickness of iron disks in endcaps	250, 600 and 600 mm
Mass of iron in each endcap	2000 t
Total mass of iron in return yoke	10 000 t

because they have to transmit the large magnetic axial force corresponding to 14 700 t, without allowing local displacements due to possible gaps. These displacements can be partially converted into heat, causing a premature quench. A construction method which involved the machining of the upper surface of the modules and a local resin impregnation during the mechanical mounting allowed us to get an excellent mechanical coupling between the modules.



Figure 2.2: The cold mass mounted vertically before integration with thermal shields and insertion in the vacuum chamber.

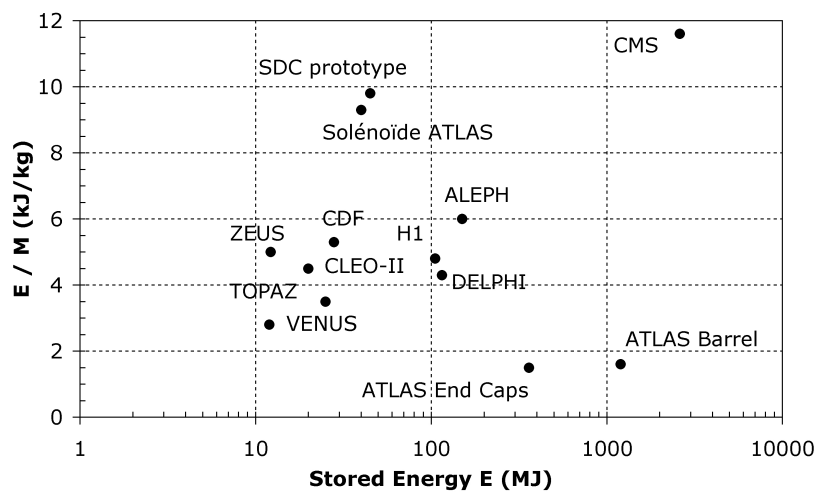


Figure 2.3: The energy-over-mass ratio E/M , for several detector magnets.

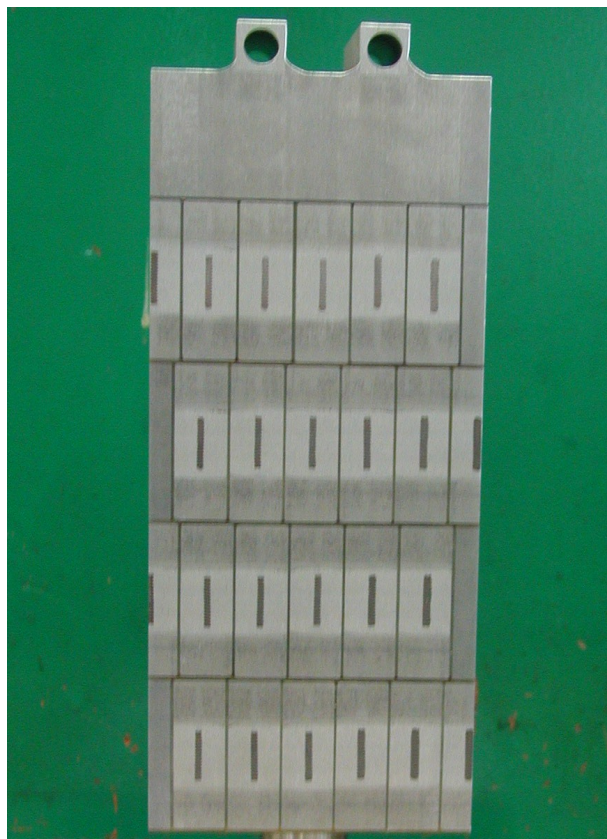


Figure 2.4: Cross section of the cold mass with the details of the 4-layer winding with reinforced conductor.

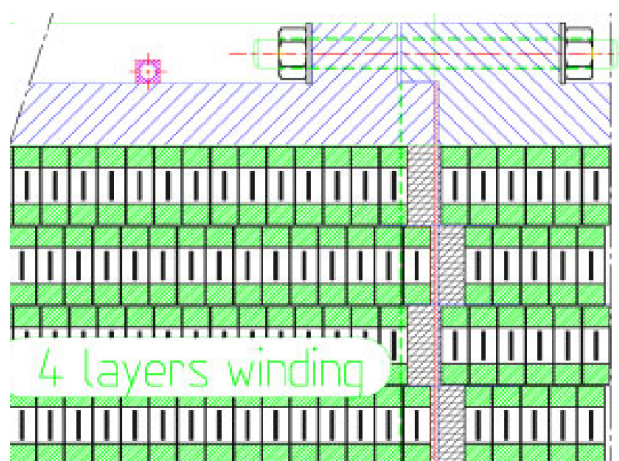


Figure 2.5: Detail of the interface region between 2 modules. In order to guarantee mechanical continuity, false turns are involved. The modules are connected through bolts and pins fixed through the outer mandrels.



Figure 2.6: A view of the yoke at an early stage of magnet assembly at SX5. The central barrel supports the vacuum chamber of the superconducting coil. At the rear, one of the closing end cap disks is visible.

2.2.2 Yoke

The yoke (figure 2.6) is composed of 11 large elements, 6 endcap disks, and 5 barrel wheels, whose weight goes from 400 t for the lightest up to 1920 t for the central wheel, which includes the coil and its cryostat. The easy relative movement of these elements facilitates the assembly of the sub-detectors. To displace each element a combination of heavy-duty air pads plus grease pads has been chosen. This choice makes the system insensitive to metallic dust on the floor and allows transverse displacements. Two kinds of heavy-duty high-pressure air pads with a capacity of either 250 t (40 bars) or 385 t (60 bars) are used. This is not favourable for the final approach when closing the detector, especially for the YE1 endcap that is protruding into the vacuum tank. A special solution has been adopted: for the last 100 mm of approach, flat grease-pads (working pressure 100 bar) have been developed in order to facilitate the final closing of the detector. Once they touch the axially-installed z-stops, each element is pre-stressed with 100 t to the adjacent element. This assures good contact before switching on the magnet. In the cavern the elements will be moved on the 1.23% inclined floor by a strand jacking hydraulic system that ensures safe operation for uphill pulling as well as for downhill pushing by keeping a retaining force. The maximum movements possible in the cavern are of the order of 11 meters; this will take one hour.

To easily align the yoke elements, a precise reference system of about 70 points was installed in the surface assembly hall. The origin of the reference system is the geometrical center of the coil. The points were made after loading the coil cryostat with the inner detectors, the hadronic barrel in particular which weights 1000 t. A mark on the floor was made showing the position of each foot in order to pre-position each element within a ± 5 mm tolerance. Finally, all the elements were aligned with an accuracy of 2 mm with respect to the ideal axis of the coil.

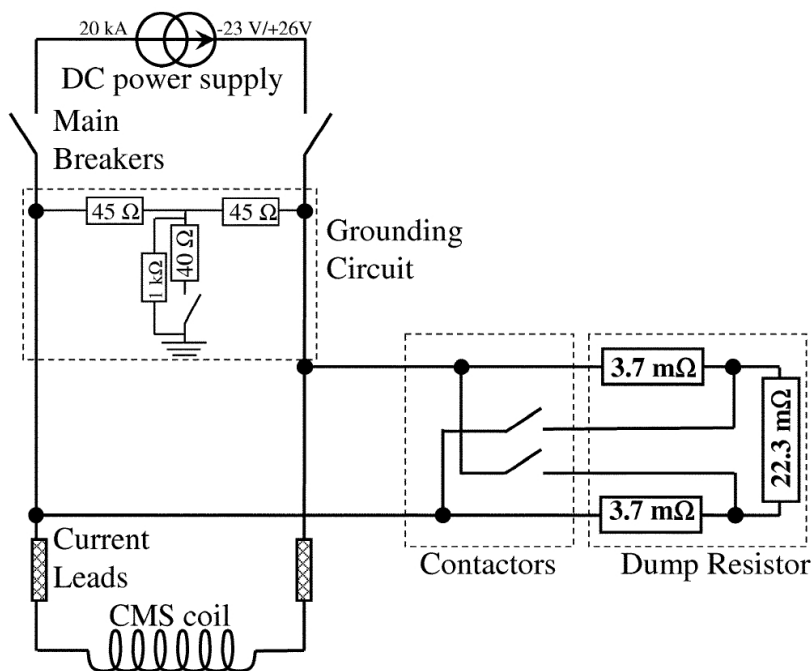


Figure 2.7: The electrical scheme of the magnet with the protection circuit. One of the main components of the protection is the dump resistor, made of three elements.

2.2.3 Electrical scheme

The CMS solenoid can be represented as a 14 H inductance mutually coupled with its external mandrel. This inductive coupling allows for the so-called *quench back* effect, as the eddy currents, induced in the external mandrel at the trigger of a current fast discharge, heat up the whole coil above the superconducting critical temperature. This is the fundamental basis of the protection system, which, in case of a superconducting to resistive transition of the coil, aims at keeping the lowest possible thermal gradients and temperature increase in the superconducting windings, and prevents the occurrence of local overheating, hence reducing the thermal stresses inside the winding. A diagram of the powering circuit with protection is shown in figure 2.7.

A bipolar thyristor power converter rated at 520 kW with passive L-C filters is used to power the CMS solenoid. It covers a range of voltages from +26 V to -23 V, with a nominal DC current of 19.1 kA. In case of a sudden switch off of the power converter, the current decays naturally in the bus-bar resistance and through the free-wheel thyristors until the opening of the main breakers. Inside the power converter, an assembly of free-wheel thyristors, mounted on naturally air-cooled heat sinks, is installed. In case of non-opening of the main switch breakers, the thyristors are rated to support 20 kA DC for 4 minutes. The current discharge is achieved by disconnecting the electrical power source by the use of two redundant 20 kA DC normally-open switch breakers, leaving the solenoid in series with a resistor, in a L-R circuit configuration. The stored magnetic energy is therefore extracted by thermal dissipation in the so-called dump resistor. This resistor is external to the solenoid cryostat and is designed to work without any active device. It is positioned

outdoors taking advantage of natural air convection cooling. The fast discharge (FD) is automatically triggered by hardwired electronics only in case of a superconductive-to-resistive transition, a so-called quench, and for unrecoverable faults which require fast current dumping. The FD time constant is about 200 s. An emergency FD button is also available to the operator in case of need. As the coil becomes resistive during the FD, energy is dissipated inside the coil, which heats up. As a consequence, this necessitates a post-FD cool-down of the coil. The FD is performed on a 30 m Ω dump resistor, as a compromise to keep the dump voltage lower than 600 V, and to limit the coil warm-up and subsequent cool-down time. For faults involving the 20 kA power source, a slow discharge (SD) is triggered through hardwired electronics on a 2 m Ω dump resistor. The SD current evolution is typically exponential, and its time constant is 7025 s, but the coil stays in the superconducting state as the heat load, about 525 W, is fully absorbed by the cooling refrigerator. For current lower than 4 kA, a FD is performed in any case, as the heat load is small enough for the refrigerator. The same resistor is used in both cases for the FD and the SD, using normally open contactors, leaving the dump resistor modules either in series (FD) or in parallel (SD). For other cases, and depending on the alarms, the coil current can be adjusted by the operator, or ramped down to zero, taking advantage of the two-quadrant converter.

2.2.4 Vacuum system

The vacuum system has been designed to provide a good insulation inside the 40 m³ vacuum volume of the coil cryostat. It consists of 2 double-primary pumping stations, equipped with 2 rotary pumps and 2 Root's pumps, that provide the fore vacuum to the two oil diffusion pumps located at the top of CMS and connected to the coil cryostat via the current leads chimney and the helium phase separator. The rotary pumps have a capacity of 280 m³/h while the two Root's pumps have a flow of 1000 m³/h. The biggest oil diffusion pump, installed via a DN 400 flange on the current leads chimney, has a nominal flow of 8000 l/s at 10⁻⁴ mbar of fore vacuum. The smallest one delivers 3000 l/s at the phase separator.

2.2.5 Cryogenic plant

The helium refrigeration plant for CMS is specified for a cooling capacity of 800 W at 4.45 K, 4500 W between 60 and 80 K, and simultaneously 4 g/s liquefaction capacity. The primary compressors of the plant have been installed, in their final position, while the cold box, as well as the intermediate cryostat which interfaces the phase separator and the thermo-syphon, were moved underground after the completion of the magnet test. These components were commissioned with the help of a temporary heat load of 6.5 kW that simulated the coil cryostat which was not yet available. The performance of the cold box has been measured in cool-down mode and in nominal and operation mode.

2.2.6 Other ancillaries

- *Current leads.* The two 20-kA current leads are made of a high purity copper braid, having a cross section of 1800 mm² and RRR (Residual Resistivity Ratio) of 130, placed inside a conduit and cooled by circulating helium gas. Without cooling, the current leads are able

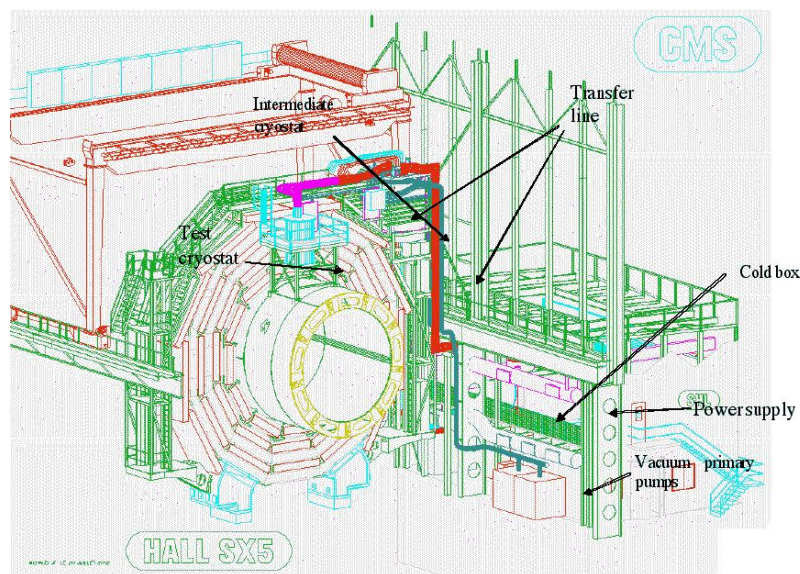


Figure 2.8: The layout for the surface test at SX5, showing only the central barrel. The magnet is connected to the cryoplant (through the proximity cryogenics), the vacuum and the power systems.

to hold a current of 20 kA for 5 minutes, followed by a FD without any damage, as the temperature at the hot spot stays below 400 K [14].

- *Grounding circuit.* The grounding circuit is connected across the solenoid terminals. It fixes the coil circuit potential, through a 1 k Ω resistor, dividing by two the potential to ground. The winding insulation quality is monitored by continuously measuring the leakage current through a 10 Ω grounding resistor.
- *Quench detection system.* The quench detection system is a key element of the Magnet Safety System (MSS). The role of the quench detection system is to detect a resistive voltage between two points of the coil, whose value and duration are compared to adjustable thresholds. The voltage taps are protected by 4.7 k Ω , 6 W resistors. There are 2 redundant systems, with resistor bridge detectors and differential detectors. For each system, there are 5 detectors. Each resistor bridge detector spans two modules and one detector spans the whole solenoid. Each coil module is compared with two other modules through two differential detectors.

2.3 Operating test

The magnet and all its ancillaries were assembled for testing in SX5 and ready for cool-down in January 2006. Figure 2.8 shows the test layout.

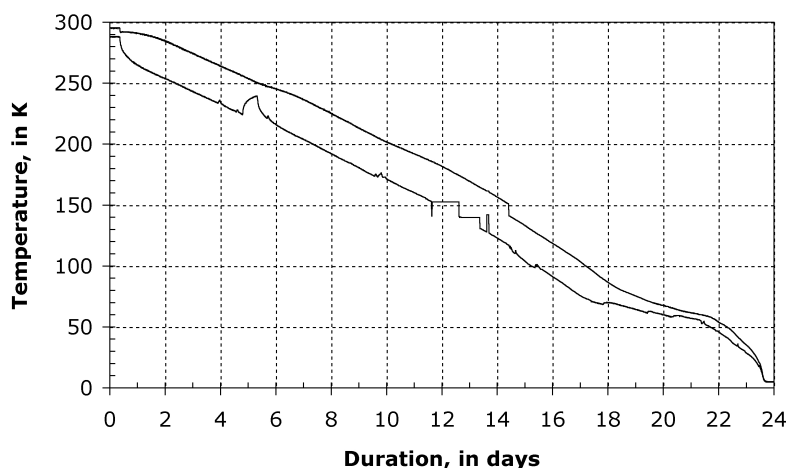


Figure 2.9: Graph of the coil minimum and maximum temperatures during the cool-down from room temperature to 4.5 K.

2.3.1 Cool-down

The cool-down of the solenoid started on February, the 2nd, 2006 and in a smooth way brought the cold mass to 4.6 K in 24 days. Figure 2.9 shows the cool-down curve. The only glitch was due to an overpressure on a safety release valve that stopped cooling for one night before the system was restarted.

One important aspect monitored during the cool-down was the amount of coil shrinkage. In order to explain this point, we refer to the coil suspension system inside the cryostat (figure 2.1), made of longitudinal, vertical, and axial tie-rods in Ti alloy. The magnet is supported by 2×9 longitudinal tie rods, 4 vertical tie rods, and 8 radial tie rods. The tie rods are equipped with compensated strain gauges to measure the forces on 2×3 longitudinal, plus the vertical and radial tie rods. The tie rods are loaded in tension and flexion. To measure the tension and flexion strain, 3 strain gauges are placed on the tie rods at 0° , 90° , and 180° .

The measured stresses in the tie bars due to the cool-down, causing a shrinkage of the cold mass and putting the tie-bars in tension, are shown in table 2.2. A comparison with the expected values is provided as well. The measured axial and radial shrinkage of the cold mass is shown in figure 2.10.

2.3.2 Charge and discharge cycles

The magnetic tests took place during August 2006, with additional tests during the magnet field mapping campaign in October 2006. The current ramps for the field mapping are detailed in figure 2.11. The tests were carried out through magnet charges to progressively higher currents, setting increasing dI/dt , followed by slow or fast discharges. During these current cycles all the relevant parameters related to electrical, magnetic, thermal, and mechanical behaviours have been

Table 2.2: Calculated and measured cold mass displacements and related stresses on tie-rods due to the cool-down to 4.5 K.

	Expected value	Measured value
Cold Mass Shrinkage		
Longitudinal	26 mm	27 mm
Radial	14 mm	15 mm
Tie rod stress due to cool-down		
Vertical	315 MPa	310±45 MPa
Radial	167 MPa	153±20 MPa
Longitudinal	277 MPa	260±20 MPa

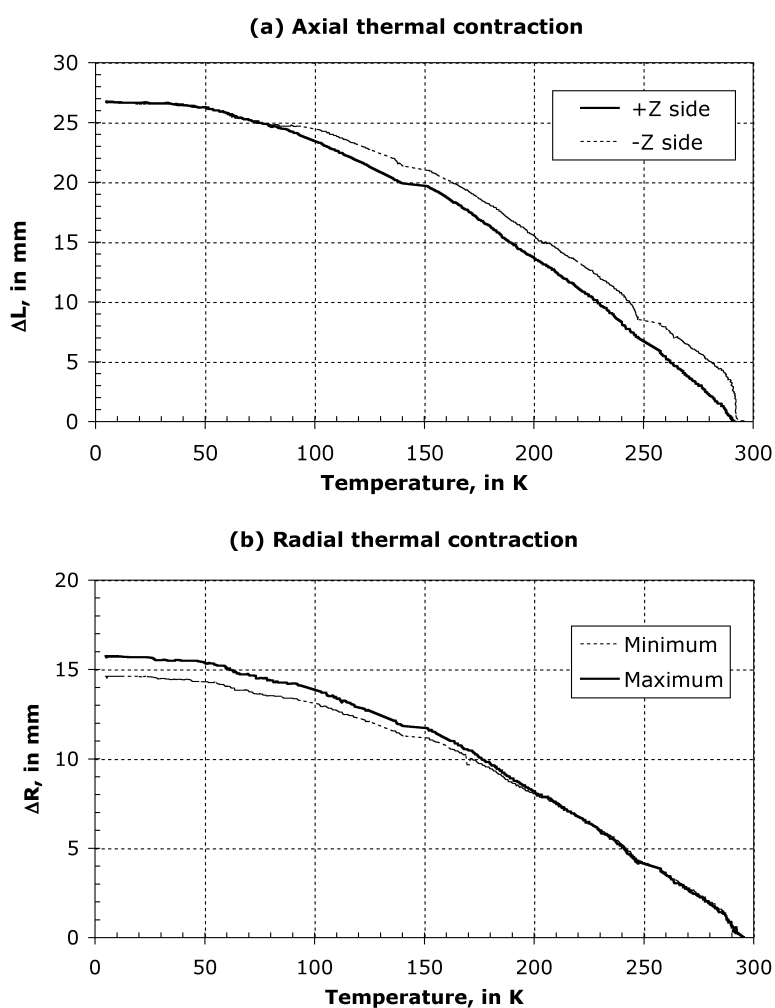


Figure 2.10: Axial (a) and radial (b) shrinkage of the cold mass from 300 K to 4.5 K.

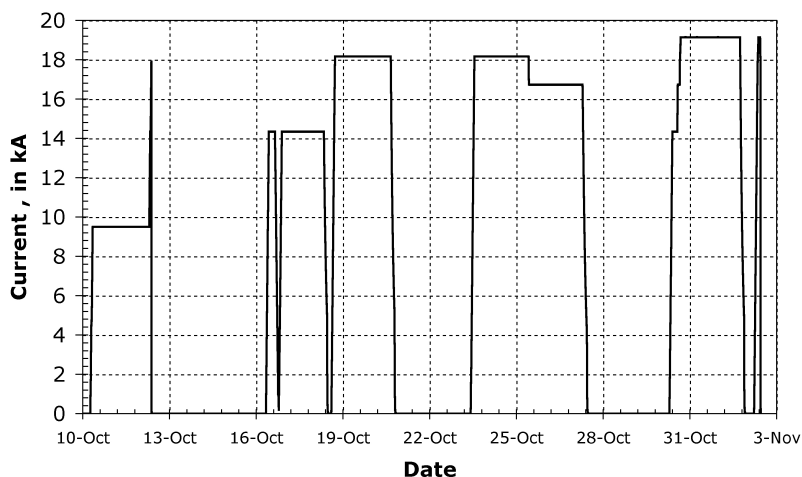


Figure 2.11: Magnet cycles during the CMS magnet tests in October 2006.

recorded. Depending on the level of the current at the trigger of a fast discharge, the time needed for re-cooling the coil can be up to 3 days.

2.3.3 Cold mass misalignment

The support system is designed to withstand the forces created by a 10 mm magnetic misalignment, in any direction of the cold mass with respect to the iron yoke. Geometrical surveys were performed at each step of the magnet assembly to ensure a good positioning. Nevertheless, the monitoring of the coil magnetic misalignment is of prime importance during magnet power test. The misalignment can be calculated either by analysing the displacement of the cold mass or the stresses of the tie rods when the coil is energised. The displacement is measured at several locations and directions at both ends of the coil with respect to the external vacuum tank wall, by the use of rectilinear potentiometers. Results are displayed in figures 2.12 and 2.13. The displacement of the coil's geometric centre is found to be 0.4 mm in z , in the $+z$ direction. According to the computations, such a displacement indicates that the coil centre should be less than 2 mm off the magnetic centre in $+z$. As the coil supporting system is hyper-static, the tie rods are not all initially identically loaded. But the force increase during energising is well distributed, as shown in figure 2.14 and figure 2.15, giving the force measurements on several tie rods. These figures also indicate the forces computed in the case of a 10-mm magnetic misalignment, together with forces calculated for the ideally-centred model, showing there is no noticeable effect of misalignment on the forces.

Using the strain gauges glued on the cold mass (outer mandrel of the central module, CB0), one can determine the Von Mises stress. The cold mass Von Mises stress versus the coil current is given in figure 2.16. The measured value of Von Mises stress at 4.5 K and zero current is 23 MPa. The value at 19.1 kA is 138 MPa. These values are in agreement with computations done during design [3, 6].

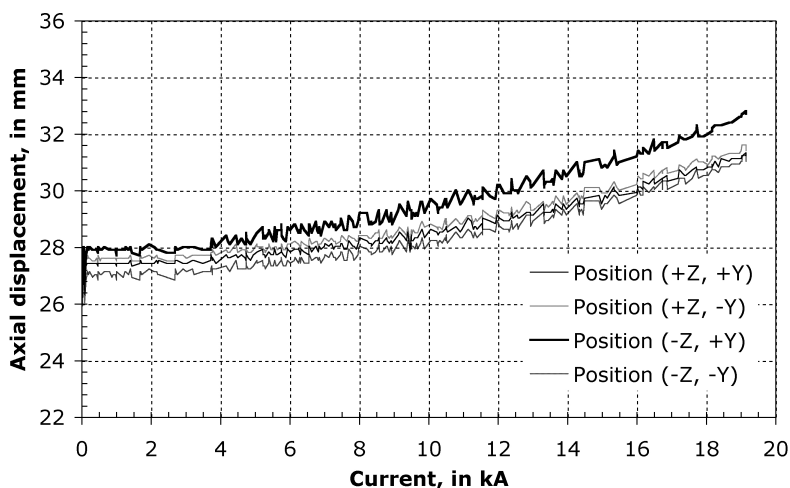


Figure 2.12: Axial displacement in Z at both ends of the coil in different positions during energising.

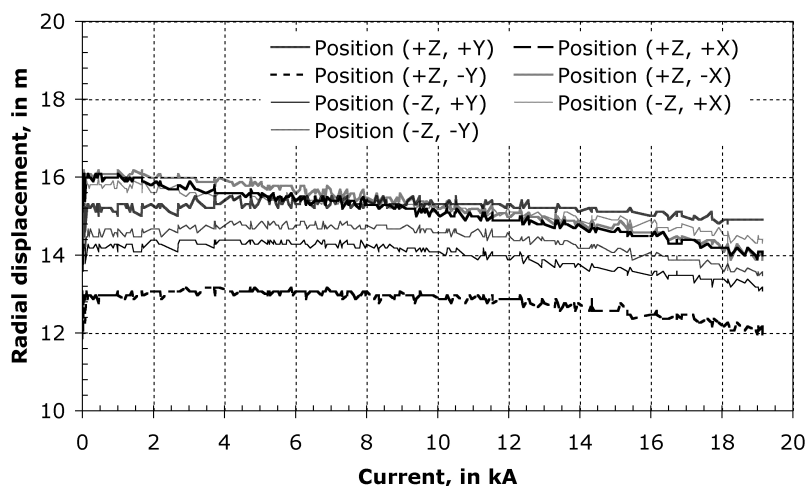


Figure 2.13: Radial displacement at both ends of the coil in different positions during energising.

2.3.4 Electrical measurements

The apparent coil inductance measured through the inductive voltage $V = LdI/dt$ is decreasing while increasing the current, as the iron yoke reaches the saturation region. From voltage measurements at the coil ends in the cryostat, while ramping up the coil current at a regulated dI/dt , the inductance is calculated and results are given in figure 2.17. Initially the apparent inductance of the coil is 14.7 H at zero current, and then it decreases to 13.3 H at 18 kA. The 21 resistive electrical joints, which connect the 5 modules together and, for each module, the 4 layers, are positioned externally to the coil, on the outer radius of the external mandrel, in low magnetic field regions. The

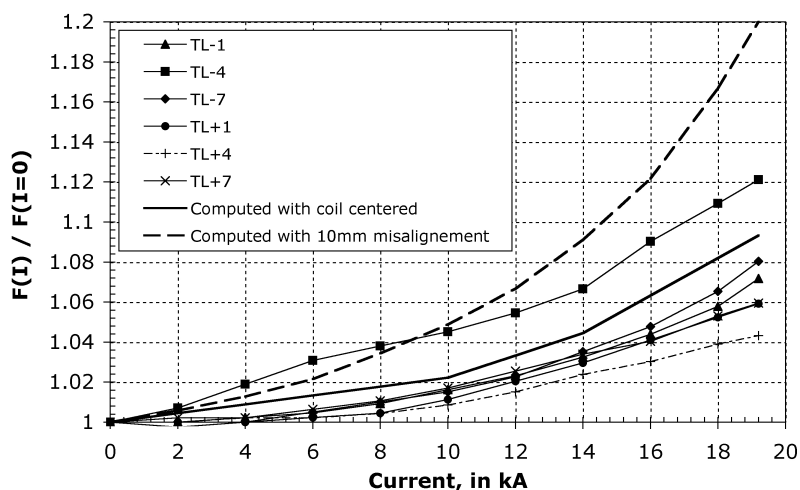


Figure 2.14: Force increase on several axial tie rods; the average force at zero current is 45 t.

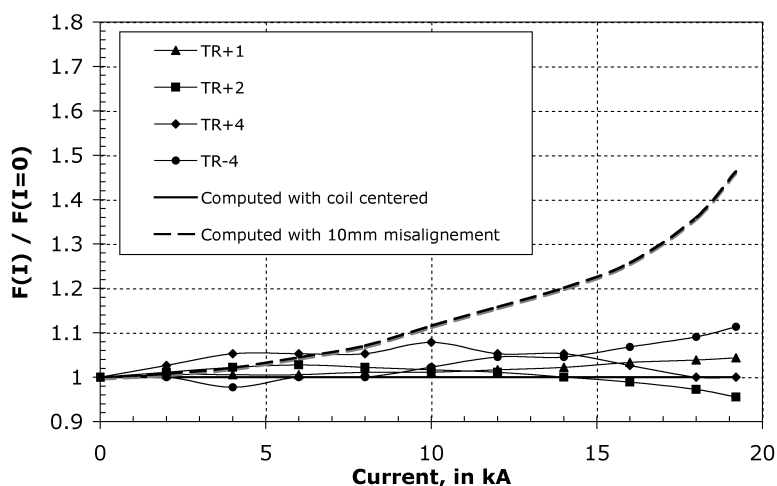


Figure 2.15: Force increase on several radial tie rods; the average force at zero current is 15 tons.

resistance measurements of the joints indicate values ranging from 0.7 n Ω to 1.6 n Ω at 19.1 kA, corresponding to a maximum dissipation in the joint of 0.6 W. The specific joint cooling system is fully efficient to remove this local heat deposit in order to avoid that the resistive joints generate a local quench of the conductor. As mentioned above, the fast discharge causes a quench of the coil, through the quench-back process. The typical current decay at the nominal current of 19.14 kA is given in figure 2.18.

The effect of the mutual coupling of the coil with the external mandrel is clearly visible at the beginning of the current fast discharge as shown in the zoomed detail of figure 2.18. It appears clearly that a high dI/dt of about 500 A/s occurs at the very beginning of the discharge. The

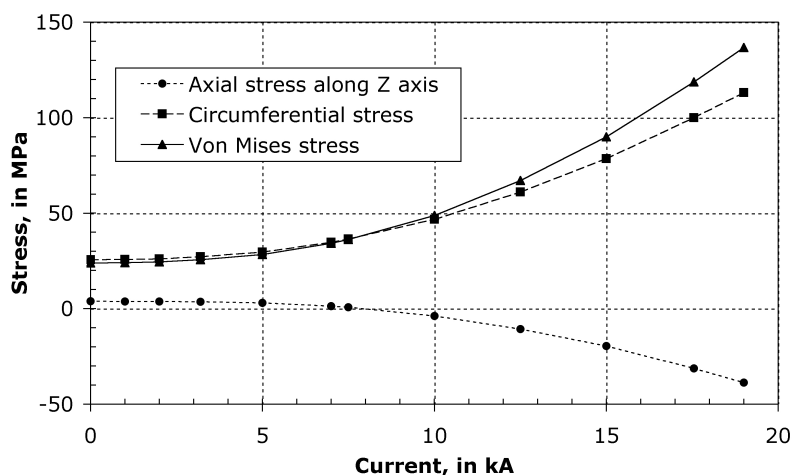


Figure 2.16: Stresses measured on the CB0 module as a function of the current.

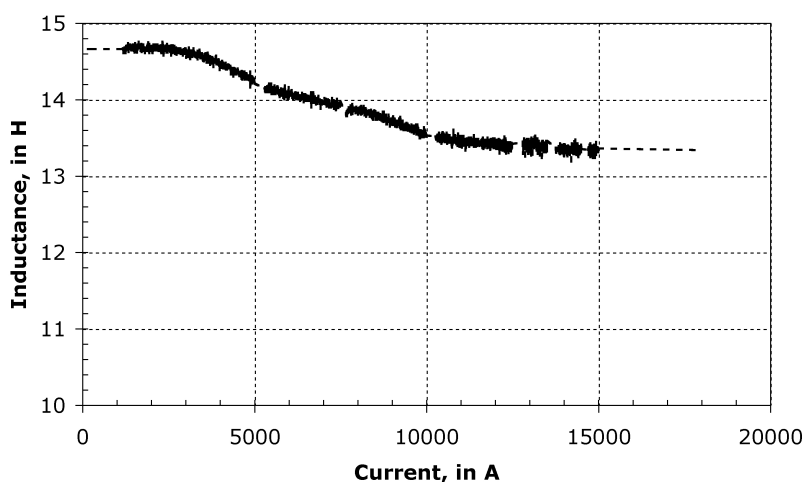


Figure 2.17: Coil inductance as a function of the magnet current.

minimum and maximum temperatures of the coil are displayed in figure 2.19 for a fast discharge at 19.14 kA. A maximum temperature difference of 32 K is measured on the coil between the warmest part, located on the coil central module internal radius, and the coldest part, located on the external radius of the mandrel. It should be noted that the thermal gradient is mainly radial. The temperature tends to equilibrate over the whole coil 2 hours after the trigger of the fast discharge. The average cold mass temperature after a fast discharge at 19 kA is 70 K.

During a magnet discharge, the dump resistor warms up, with a maximum measured temperature increase of 240°C, resulting in an increase of the total dump resistance value by up to 19%. Also the coil internal electrical resistance is increased by up to 0.1 Ω at the end of a FD at 19.14 kA.

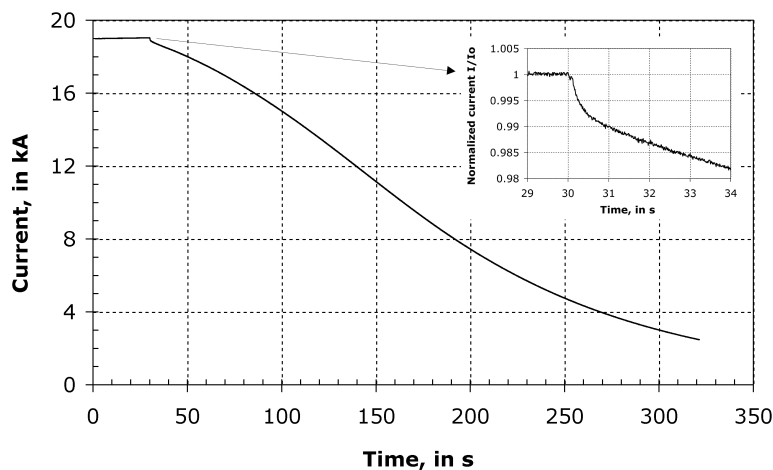


Figure 2.18: Magnet current during fast discharge at the nominal field of 4 T. The insert shows the details at the beginning of the discharge.

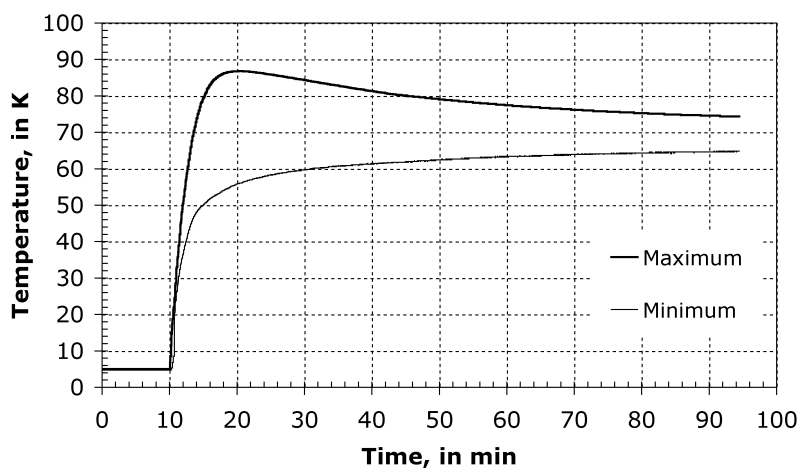


Figure 2.19: Minimum and maximum temperatures detected on the cold mass during the fast discharge from 19.1 kA.

The effect of both the dump resistor and the magnet electrical resistance increasing was revealed through the measurement of the discharge time constant, which was equal to 177 s, 203 s, 263 s, 348 s and 498 s for fast discharges respectively at 19 kA, 17.5 kA, 15 kA, 12.5 kA and 7.5 kA. This is visible in figure 2.20. The temperature recovery of the dump resistor is achieved in less than 2 hours after the trigger of a fast dump. It is 5 hours after the trigger of a slow dump.

In the case of a fast dump at 19.14 kA, typically half of the total energy (1250 MJ) is dissipated as heat in the external dump resistor. The energy dissipated in the dump resistor as a function of the

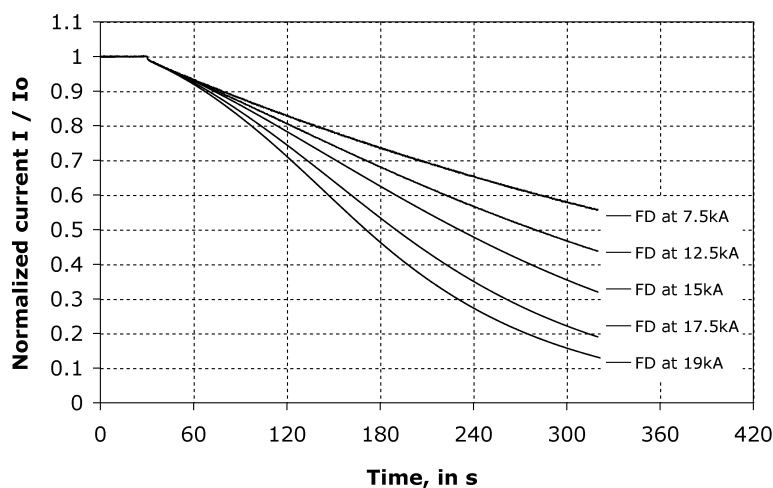


Figure 2.20: The normalised discharge current as a function of time for different initial currents, showing the effect of the increase in magnet and external dump resistance with current.

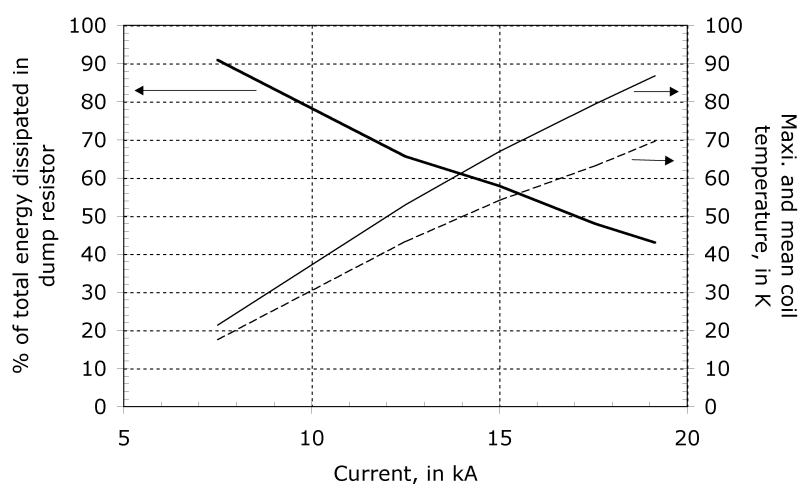


Figure 2.21: Energy dissipated in the external dump resistor and the mean and maximum temperatures of the coil during FD.

magnet current at the trigger of a FD was measured for each FD performed during the magnet tests and is given in figure 2.21. The magnet current is precisely measured by the use of two redundant DCCTs (DC current transformer). The peak-to-peak stability of the current is 7 ppm with a voltage ripple of 2.5% (0.65 V). In order to gain on the operation time, an acceleration of the slow dump has been tested and validated by switching to the fast dump configuration at 4 kA. It has been checked that the cryogenic refrigerator can take the full heat load, and the magnet stays in the superconducting state. This Slow Dump Accelerated (SDA) mode was tested in semi-automatic mode through the cryogenics supervisory system and the magnet control system, and it will be fully automatic for the final installation in the cavern.

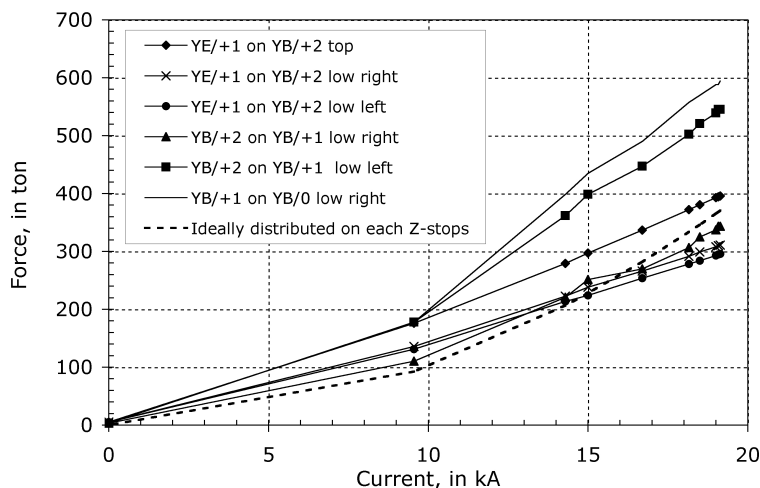


Figure 2.22: Axial forces acting on the yoke Z-stops during the coil energising.

2.3.5 Yoke mechanical measurements

The elements of the return yoke, barrels and endcaps, are attached with several hydraulic locking jacks, which are fixed on each barrel and endcap. They are pre-stressed in order to bring the barrels and endcaps into contact at specific areas using the aluminium-alloy Z-stop blocks. There are 24 Z-stops between each barrel and endcap. A computation of the total axial compressive force gives 8900 tons. The stresses are measured on some Z-stops; the forces on these Z-stops are given in figure 2.22 and compared to the case of a uniformly distributed load on all the Z-stops. To allow for uniform load distribution and distortion during magnet energising, the yoke elements are positioned on grease pads. During magnet energising, the displacement of the barrel yoke elements under the compressive axial force is very limited, while the displacement of the yoke end cap disk YE+1 is clearly noticeable on the outer radius of the disk, due to the axial attraction of the first yoke endcaps towards the interaction point. The measurement of the distance between the barrel elements parallel to the axial axis of the detector is given in figure 2.23. The endcap YE+1 disk is equipped with rosette strain gauges on its inner face, under the muon chambers and near the bolts at the interface between two adjacent segments. The main stresses measured in these regions do not exceed 88 MPa.

2.3.6 Coil stability characteristics

The NbTi superconductor critical temperature is $T_c = 9.25$ K at zero field. At $B = 4.6$ T (peak field on the conductor), $T_c = 7.30$ K. The current-sharing temperature T_g is defined as the maximum temperature for which the current can flow, with no dissipation, in the superconducting part. For CMS the operating current is 19 143 A, while the critical current, according to the measurements done on a short sample extracted from the length used in the inner layer of the central module (the one exposed to the higher field), is $I_c (T = 4.5$ K, $B = 4.6$ T) = 62 kA leading to $T_g = 6.44$ K, i.e., the temperature margin is 1.94 K. This margin is a little higher than the designed one (1.83

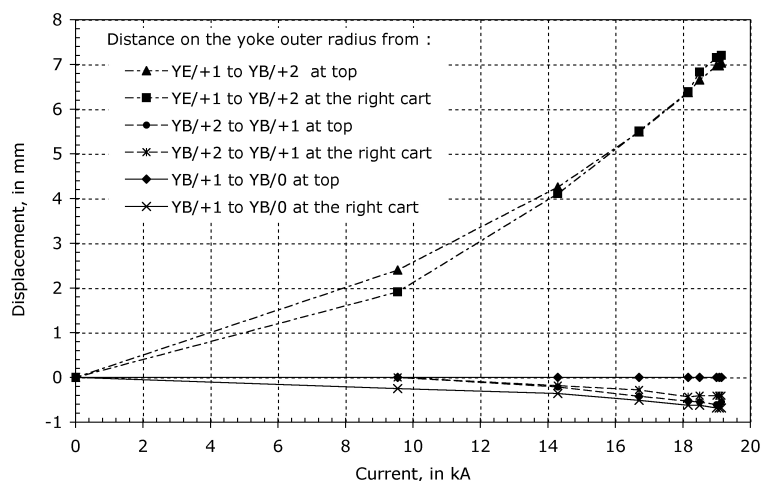


Figure 2.23: Measured displacement of the yoke during the coil energising.

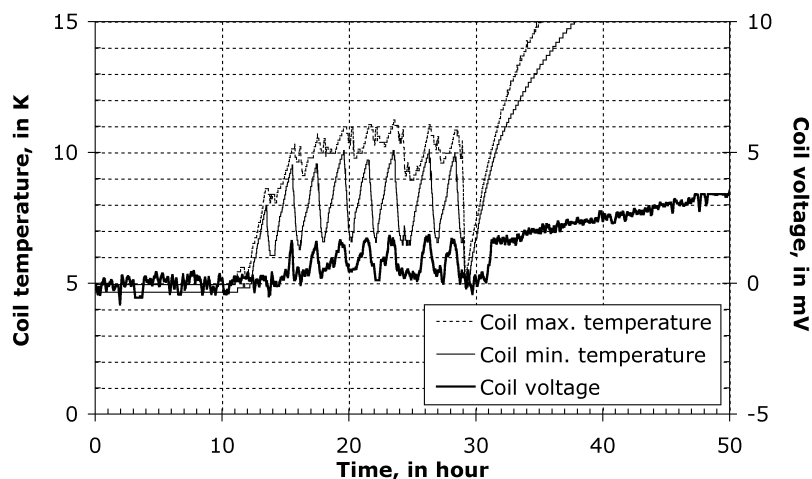


Figure 2.24: The minimum and maximum temperatures and voltage of the coil as a function of time, with only a few amperes of current, showing the superconducting-to-resistive-state transition at around 9.3 K.

K) because the nominal current is less than the one used in this kind of computation (19.5 kA) and the expected conductor critical current was from 7% to 10% lower than the real one obtained through advanced and qualified processes. The T_c value was confirmed at 9.3 K during cryogenic recovery tests (figure 2.24) at zero field. The conductor pure-aluminium stabilizer RRR, deduced from electrical measurements during cool-down, is found to be above 1800.

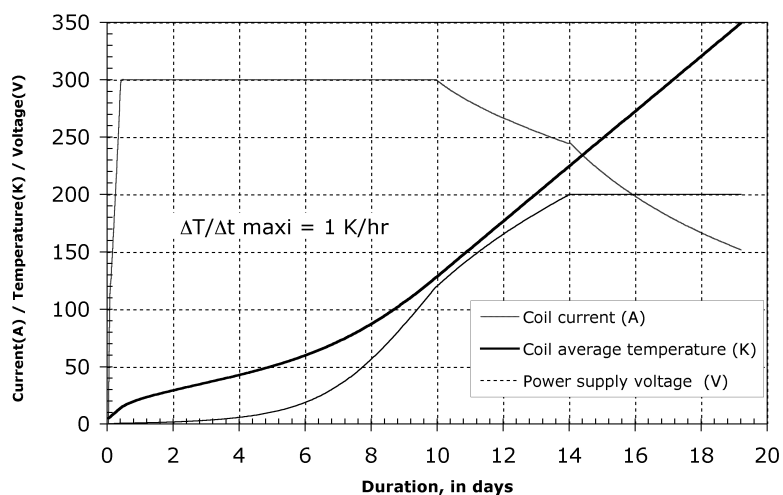


Figure 2.25: Measurements of the coil warm-up behaviour as a function of time; the Y-axis scale is common for all the three curves.

2.3.7 Coil warm-up

Following the test of the magnet on the surface, the cold mass had to be warmed up to room temperature before lowering. The coil, inside its cryostat, was attached to the central barrel YB0 to avoid any risk due to vacuum degradation during the transport operations. The warm-up was performed using a dedicated power supply (200 V-300 A DC) to maintain integrity of the coil/mandrel interface. Knowing the temperature dependence of both the electrical resistivity and the specific heat of the coil materials, the temperature increase for a given electrical power is calculated. Taking into account the capacity of the warm-up supply, and limiting the temperature increase to 1 K/hour, the warm-up was performed as shown in figure 2.25. As the warm-up was done after a fast discharge, the coil temperature was already at 70 K. Nevertheless, the warm-up took place only at night as the yoke was opened to continue integration activities inside the detector. Ultimately, the warm-up lasted only 3 weeks. The maximum temperature gradient across the coil during the warm-up exercise was less than 9 K.